

# **Microstructure controls physical properties of smectite clay**

**Roland Pusch<sup>1</sup>**

## **Abstract**

Environmental protection by isolation of radionuclides escaped from High-Level Radioactive Waste stored underground in crystalline rock can be achieved by surrounding the metal canisters by smectite clay, which provides hindrance of radionuclides to migrate into the surroundings, and ductile embedment of them for absorbing seismic and tectonic displacements in the host rock. The waste-isolating capacity of the expansive clay is explained by its high hydrophilic capacity and large specific surface area giving low porosity and limited interconnectivity of the voids, which both makes such clay low-permeable and gives it a very low through-diffusion rate of anionic species like iodine, and of some cationic radionuclides. The expandability of such clay means that it can swell and undergo self-healing in case of microstructural contraction caused by heating. The mechanisms involved in permeation and ion exchange are described based on conceptual microstructural models and their theoretical analogies. Stress/strain phenomena involved in saturation with fluids, desiccation, shearing under deviatoric conditions, and creep strain under stable conditions or at failure are described as well. Longevity matters, which have been richly treated in the literature, is given limited space.

**Keywords:** Smectite clay, montmorillonite, microscopy, clay microstructure.

## **1. Scope of study**

---

<sup>1</sup> Luleå University of Technology, Sweden

Disposal of radioactive waste is suitably made underground in stable crystalline rock at several hundred- or thousand-meters depth, utilizing the host rock for mechanical protection, and engineered barriers of clay for limiting migration of radionuclides to the surroundings of the repository. In this document we consider the performance of smectite clay with respect to migration of radionuclides emanating from stored highly radioactive waste, like spent nuclear fuel.

## 2. Smectite clay

### 2.1 Crystals

The basic units consist of stacked lamellae each of them consisting of two sheets of  $\text{SiO}_4$  tetrahedrons confining a central octahedral layer of hydroxyls and Fe, Mg or Li ions (Figure 1). These minerals belong to the group known as:

- *Montmorillonite*: Only Si in the tetrahedrons and Al in the octahedrons
- *Beidellite*: Si and Al in the tetrahedrons and Al in the octahedrons
- *Nontronite*: Si and Al in the tetrahedrons and Fe in the octahedrons
- *Hectorite*: Si in the tetrahedrons and Mg and Li in the octahedrons
- *Saponite*: Si and Al in the tetrahedrons and Mg in the octahedrons

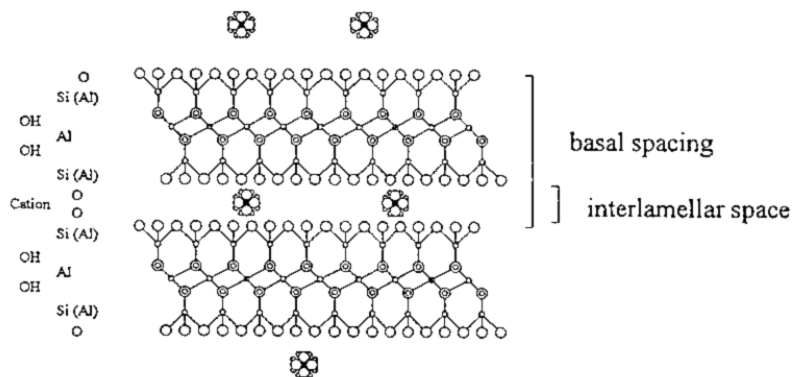


**Figure 1: Smectite lamella in weakly hydrated state, with 1 nm thickness. The interlamellar space can host water and cations.**

Figure 2 shows how the crystal constituents join to form smectite lamellae. Forces keeping the lamellae together are weak allowing for easy separation of them.

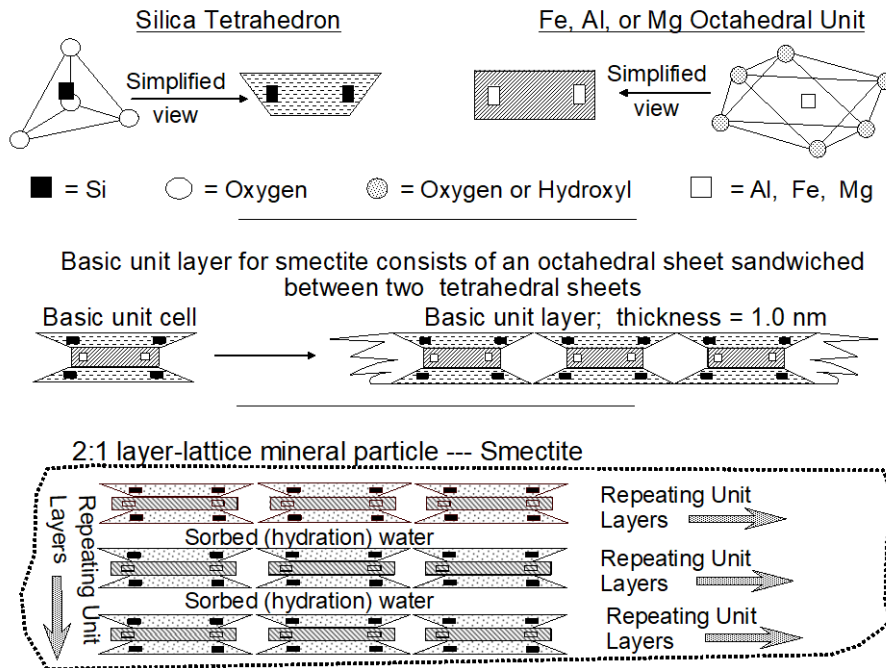


**Figure 2: Stacking of unit layers with the interlamellar space occupied with hydration water (After Yong). This space is often termed “internal” for distinguishing it from the “external” space between particles, i.e. stacks of lamellae.**

## 2.2 Particles

The stacks represent clay particles, which are more or less interwoven in undisturbed natural smectite clays like “bentonites” having been formed from volcanic glass deposited in salt water. This interwoven nature makes it difficult to define the particle size and shape and results in a large variation in size distribution depending on sample procurement and testing. Smectite particles have a peculiar shape and appear in networks that make it difficult to identify individual members and to define and measure their size and shape (Figure 3).

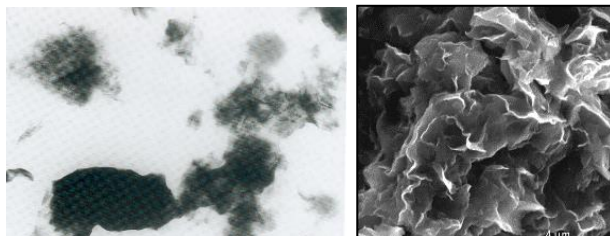


**Figure 3: Montmorillonite particles. Left: transmission electron micrograph (TEM) of aggregated crystallites with a maximum size of about 0.5  $\mu\text{m}$ . An illite particle with about 1  $\mu\text{m}$  length is seen in the lower left of the graph (dark). Right: scanning micrograph (SEM) of soft montmorillonite clay.**

### 2.3 Interlamellar hydration of smectite particles

The hydration of the interlamellar space depends on the charge and coordination of adsorbed cations and water molecules Pusch (2015). A water hull, one monolayer thick and containing cations, is sorbed on the basal surfaces of practically all minerals, and plays a role in diffusive ion transport and in osmotic swelling of smectites. The interlamellar hydrates determine the swelling potential, while the hydrated surface properties of the stacks of lamellae determine the bulk plasticity and rheological behaviour.

The coordination of interlamellar water molecules and cations and the crystal lattice atoms depends on the size and charge of the cations and of the charge distribution in the lattice. Three hydrate layers can only be formed in some of the smectite species, and normally only when sodium, lithium or magnesium are in interlamellar positions (Table 1). One finds from this table that montmorillonite is the only smectite mineral of the listed ones that can expand to form 3 interlamellar hydrates.

**Table 1: Number and thickness of interlamellar hydrates in nm (Kehres, 1983).**

| Smectite clay                    | M <sup>1</sup> | 1st hydrate | 2nd hydrate | 3rd hydrate |
|----------------------------------|----------------|-------------|-------------|-------------|
| Montmorillonite                  | Mg             | 0.30        | 0.30        | 0.30        |
|                                  | Ca             | 0.39        | 0.28        | -           |
|                                  | Na             | 0.30        | 0.32        | 0.35        |
|                                  | K              | 0.24        | 0.37        | -           |
| Beidellite                       | Mg             | 0.27        | 0.27        | -           |
|                                  | Ca             | 0.23        | 0.23        | -           |
|                                  | Na             | 0.22        | 0.22        | -           |
|                                  | K              | 0.25        | -           | -           |
| Nontronite                       | Mg             | 0.29        | 0.30        | -           |
|                                  |                |             |             |             |
|                                  | Ca             | 0.31        | 0.34        | -           |
|                                  | Na             | 0.27        | 0.28        | -           |
|                                  | K              | 0.26        | -           | -           |
| 1: Interlamellar adsorbed cation |                |             |             |             |

Hydration proceeds until the maximum number of interlamellar hydrates are formed if there is no geometrical restraint. In humid air the number of hydrates developed depends on the relative humidity as shown by Table 2: one interlamellar hydrate is formed in Na montmorillonite when RH is in the interval 20-40 %, while two hydrates require  $40 < RH < 60$  %. For RH exceeding about 60-70 % three interlamellar hydrates can be formed. For Ca it is different (Figure 4). According to XRD testing interlamellar water forms a two-layer hydrate in Ca montmorillonite (Sposito, 1984).

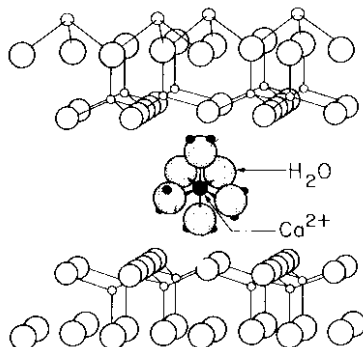


**Figure 4: Interlamellar Ca ion complex with water molecules strongly attached to the cation and interacting also with the siloxane oxygens (Sposito, 1984).**

**Table 2: d-spacing and water absorption of Na montmorillonite in atmosphere with different relative humidity (RH).**

| <b>RH %</b> | <b>Adsorption area, m<sup>2</sup>/g solids</b> | <b>d(001) spacing, Å</b> | <b>Water adsorption in g/g solids, %. Pure clay</b> | <b>Water adsorption in g/g solids, %. MX-80</b> |
|-------------|--|--------------------------|---|---|
| 14          | 33   | 10                       | 4.5   | 3.2   |
| 19          | 33   | 10                       | 6.5   | 4.6   |
| 24          | 440  | 12.4                     | 8.0   | 5.6   |
| 38          | 440  | 12.6                     | 11.5  | 8.1   |
| 60          | 810  | 14.2                     | 17.0  | 12.0  |
| 70          | 810  | 15.0                     | 21.5  | 15.0  |
| 80          | 810  | 15.2                     | 24.0  | 17.0  |
| 90          | 810  | 15.4                     | 28.0  | 20.0  |
| 95          | 810  | 15.4                     | 36.5  | 26.0  |

There is no general consensus concerning the structure of interlamellar water when Li or Na makes up the interlamellar cation. We prefer here to present Edelman/Favejee's crystal constitution in Forslind's and Jacobsson's hydrated form in Figure 5. It represents a schematic model of the organization of water molecules in the interlamellar space according to this crystal constitution of montmorillonite with Li or Na in interlamellar positions (Forslind and Jacobsson, 1972).

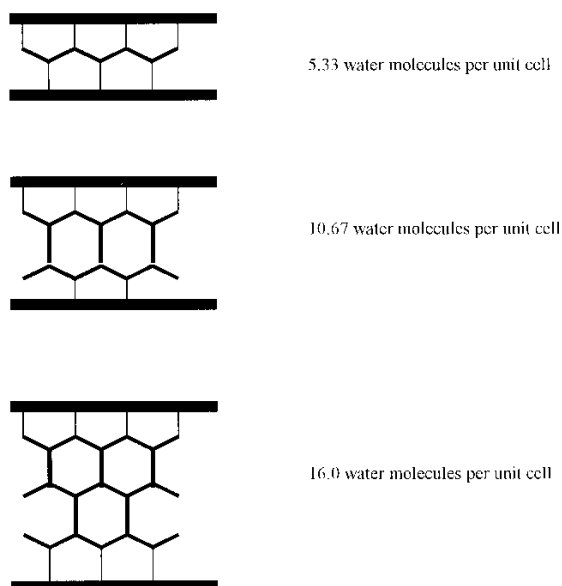


**Figure 5: Model of hydrate configuration in interlamellar montmorillonite with Edelman/Favejee's crystal constitution and interlamellar Li or Na for lower temperature than about 60°C. The stable monolayer corresponds to a d-spacing of 17.81 Å and a water content  $w=11.9\%$ , while for two layers  $d=22.41\text{ Å}$  and  $w=23.8\%$ . For three layers  $d=25.17\text{ Å}$  and  $w=35.7\%$ .**

We find from Table 1 that  $K^+$  is deeply and strongly anchored in the cavities of the siloxane (Si-O) lamella of montmorillonite because it fits geometrically and stereochemically (Sposito, 1984). Table 2 includes a column for commercial Na-dominated bentonite (MX-80), which contains about 70 % montmorillonite, the rest being rock-forming minerals. Since the water adsorption is about 70 % of that of pure Na montmorillonite their distribution is obviously uniform.

When Na is in the interlamellar space the coupling to water molecules is weak and the cations relatively free to move, which indicates that the interlamellar water molecules form their own  $H^+$ -bonded structure (Figure 5), while in Ca-smectite the cations are strongly hydrated and the interlamellar complexes rigid and stable (Figure 4). This means that the swelling pressure and the pressure required to expel interlamellar water is higher for Ca-smectite than for Na-smectite for dry bulk densities exceeding about  $1600 \text{ kg/m}^3$ . The much higher mobility of Na ions taken up from a NaCl solution is verified by the significantly higher diffusion coefficient. The water structure in the interlamellar space is still a matter of dispute but there are reasons to believe that for Li and Na in this space the crystal structure is different from that in Figure 1, implying a certain number of apical SiO tetrahedrons. It is supported by nuclear magnetic resonance investigations (“magic angle spin-echo”) that has shown an obvious difference in the co-ordination of the silicons in Na- and Ca-montmorillonite, indicating that the first mentioned is of the type in Figure 6 while the latter is as in Figure 1 (Pusch, 1993).

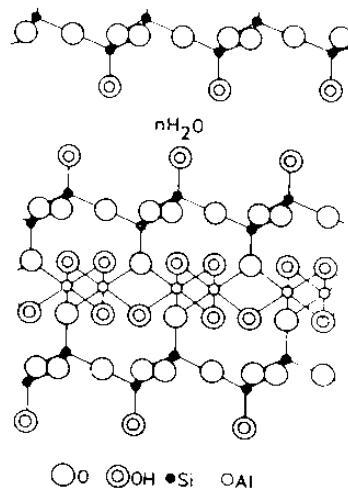


**Figure 6: Assumed crystal structure for Li- and Na-montmorillonite with apical tetrahedrons (Edelmann/Favejee/Forslind).**

From a practical point of view the different physical constitutions of interlamellar water is believed to be that the stacks of lamellae in Ca-montmorillonite, i.e. the clay “particles”, are much stronger and less easily disrupted than in Na-montmorillonite giving the first-mentioned a character of silty, frictional-type soil with less potential to form gels. Ca-montmorillonite is hence believed to be stiffer and undergo less creep strain than Na-montmorillonite exposed to the same deviator stress. In both types the interlamellar water is believed to be more viscous than ordinary water and to be largely immobile under normal hydraulic gradients.

#### **2.4 Extra lamellar hydration – hydrates on the basal planes of stacks of lamellae**

External surfaces are basal planes and edges of the stacks of lamellae. The firstmentioned consist of hexagonal arrangements of oxygens or hydroxyls and can attach water molecules by establishing hydrogen bonds (Figure 7). Where basal planes come close interacting diffuse electrical double-layers are formed with a relatively high concentration of cations near the surface, which affects the organization and physical state of the hydrates (Figure 8). Thus, it is possible that the first few hydrate layers on smectite surfaces (Water A) are more viscous than those in Water B, which are in turn less viscous than normally structured Water C. These issues are of fundamental importance for understanding diffusion processes in smectite clay.

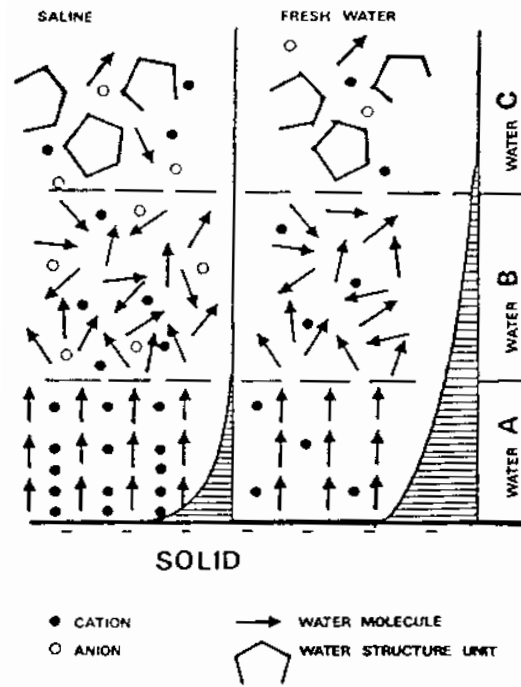


**Figure 7: Proposed organization of water and ions at clay mineral surfaces. Water A is largely immobile through coupling to surface atoms. Water B is low-viscous. Water C is free with normal viscosity. Hatched areas represent the charge distribution in the electrical double-layers (left: marine, right: fresh-water), (After Drost-Hansen).**

**Table 3: Number of hydrate layers in compacted Na montmorillonite with 1200 kg/m<sup>3</sup> dry density as a function of the water content (Colten, 1986). The clay was saturated with distilled water.**

| Water content, % (by weight) | Number of hydrates |
|------------------------------|--------------------|
| <7                           | 0                  |
| 7-10                         | 1                  |
| 10-20                        | 1-2                |
| 20-25                        | 2                  |
| 25-35                        | 2-3                |
| >35                          | 3                  |

One notices that the data are in agreement with those in Figure 5.

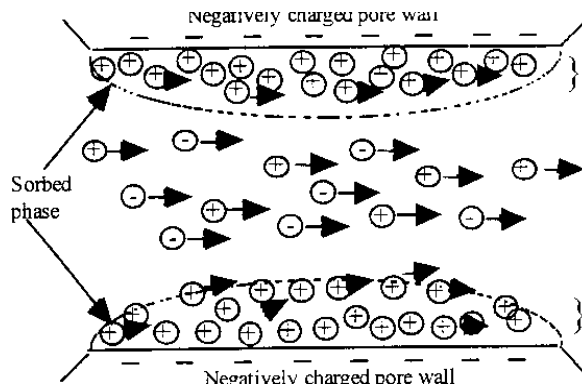


**Figure 8: Interacting electrical double-layers (Pusch et al, 1999). The intermediate space offers large amounts of hydration sites due to the crystal lattice constitution, which determines the charge and co-ordination of adsorbed cations and water.**

## 2.5 Hydration at elevated temperature and water pressure

The influence of temperature and water pressure on water sorption and particle thickness of montmorillonite clay confined in autoclaves under controlled water pressure conditions has been examined by several investigators. A carefully conducted test comprised a series of experiments on montmorillonite slurry with a fluid content of 800 % (dry density 79 kg/m<sup>3</sup>) that was placed in a cell exposed to temperatures up to 200°C and hydraulic pressures of up to 40 MPa (Colten, 1986). The molality of the NaCl solution used for saturation was 1 to 5. This study showed that the interlamellar spacing was negligibly changed in the tests, which is explained by the fact that there was no effective (“grain”) pressure acting on the clay.

A similar test series was made on MX-80 clay saturated with distilled water and enclosed in autoclave cells giving high pore water overpressures by heating. The overpressure was 40-70 MPa for temperatures up to 200°C and the swelling pressure of the clay samples, which had a dry density of 480 kg/m<sup>3</sup>, was about 70 kPa. XRD analysis of sedimented clay specimens demonstrated very small changes in interlamellar spacing, i.e. from 16.7 Å for room temperature reference samples to 16.7 to 17.3 Å spacings (001) for samples heated for 0.5 years at 150 and 200°C, respectively. These data are in fact somewhat higher than for unheated clay and confirm that no permanent contraction or compression took place under the very low effective pressures that prevailed in the course of heat treatment. However, the peak heights were increased by 5 and 50 %, respectively, indicating that alignment of stacks of lamellae were in fact caused. This process was probably generated by reorientation, compression and shearing of the stacks under the low effective pressure that actually existed. It is believed that compression of the stacks of lamellae was triggered by heat-induced reduction of the strength of the interlamellar hydrate layers.

## 2.6 The chemical potential

Generally speaking, the chemical potential of water is of fundamental importance for the build-up and performance clay soils and water with few dissolved ions has a higher chemical potential than water with solutes. The drop in potential for increasing the ion concentration can be expressed as in Eq. 2.1, (Nakano et al, 1998).

$$\mu_o = -kTC\nu \quad (1)$$

where:

$k$  = Boltzmann's constant

$T$  = Temperature

$C$  = Cation concentration in hydrates formed at mineral surfaces

$\nu$  = Partial volume of water

The cations cause polarization of neighbouring water molecules by which their mobility drops and the chemical potential is reduced. Further reduction is due to van der Waals attraction between the hydrates and adjacent mineral lattice and to hydrogen bonds established between the hydrates and lattice hydroxyls. Interlamellar hydrates are pressed together by the attraction between the lamellae, which increases the chemical potential. It is hence highest for low water contents and higher for interlamellar hydrates than for hydrates on basal surfaces of clay particles. Nakano et al found that the chemical potential of the first hydrate adsorbed on basal surfaces is on the order of  $E7$  J/kg, and about  $E2$  J/kg for hydrates at around 6 nm from the surfaces.

This theory can be used for calculating water retention curves in the form of relationships between the water content and the chemical potential (Figure 9). The values depend on the number of lamellae as illustrated by the much higher chemical potential ( $3E4$  J/kg) for the volumetric water content 20 % when the number of lamellae is 8 than when this number is 4. The water retention of dense clay is hence higher than of soft clays. Similarly, the chemical potential of the pore water is much higher of dense than of soft clay. For a water content of about 20 % the chemical potential  $E5$  J/kg corresponds to a suction of as much as 100 MPa. Molecular dynamic/homogenization theories have been used for modeling the organization of montmorillonite lamellae and interlamellar water and this has led to some interesting microstructural features (Ichilawa et al, 1998). Thus, the chemical potential decrement of the pore water due to the solute, electrical field and van der Waals forces implies that for a bulk dry density of  $1000$  kg/m<sup>3</sup> the stacks contain 4 lamellae while for a dry density of  $1800$  kg/m<sup>3</sup> this number is 8. The water adjacent to montmorillonite surfaces is concluded to be rigidly associated with the crystal lattice while further hydrates have a viscosity that drops quickly with increasing distance from the surfaces up to  $25$  Å (2.5 nm) where the viscosity is the same as for free water (Figure 9).

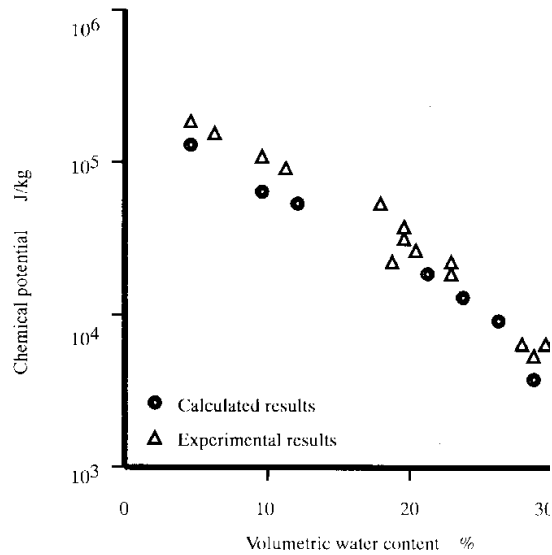


**Figure 9: Chemical potential of montmorillonite-rich clay calculated by use of molecular dynamics and determined experimentally (Nakano et al, 1998).**

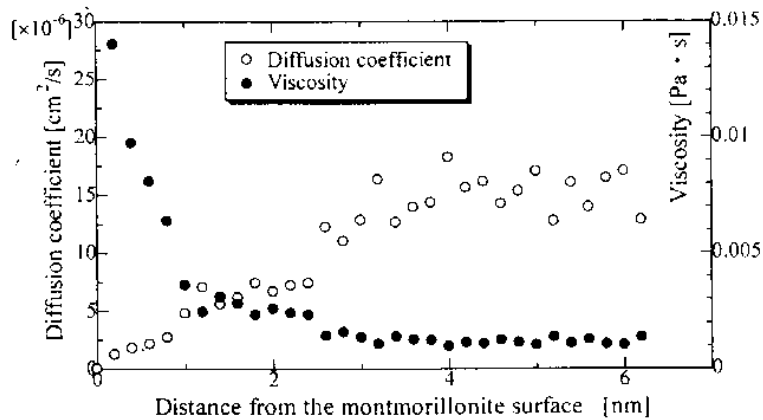


**Figure 10: Diffusion coefficient and viscosity of montmorillonite clay calculated by use of molecular dynamics (Ichikawa et al, 1998).**

A study by use of vapour pressure measurements and X-ray diffraction technique supports the conclusion that three distinct hydrate layers can be established in the interlamellar space in montmorillonite and that they are as strongly held to the clay lattice as ice although the interlamellar water is layered rather than 3D-structured (Kehres, 1983). This study led to the conclusion that the number of hydrates is related to the water content as shown in Table 3 for Na montmorillonite with a dry density of  $1200 \text{ kg/m}^3$ , corresponding to  $1750 \text{ kg/m}^3$  at complete water saturation (Pusch, R., 2012).

## 2.7 Cation sorption on smectite

The lattice charge deficit makes the smectites adsorb and exchange ions and organic molecules as manifested by the cation exchange capacity. Under a given set of conditions different cations are not equally replaceable and do not have the same replacing power. The replacing power of some typical ions are shown as a lyotropic series as follows from Grim and Gueven (1978):



The replacement positions are to a very large extent dependent on the size of the hydrated cation and on the magnitude of the electric potential where the cations are located. The proportion of each exchangeable cation to the total cation exchange capacity (CEC) is determined by the exchange-equilibrium equations, like the Gapon equation (Yong, 2001):

$$\frac{M_e^{+m}}{N_e^{+n}} = K \frac{[M_o^{+m}]_m^1}{[N_o^{+n}]_n^1} \quad (2)$$

where (i) the superscripts  $m$  and  $n$  refer to the valence of the cations, (ii) the subscripts  $e$  and  $o$  refer to the exchangeable and bulk solution ions, and (iii) the constant  $K$  is a function of specific cation adsorption and nature of the clay surface.  $K$  decreases as the surface density of charges increases.  $\text{Na}^+$  vs.  $\text{Ca}^{2+}$  represents a particularly important case of competition. Thus, it is a well-known fact that as the amount of exchangeable calcium on the clay mineral becomes less it becomes more difficult to release. Sodium, on the other hand, tends to be more easy to release as the degree of saturation with sodium ions drops.

Potassium is an exception that has been explained by geometrical measures: its ionic diameter  $2.66 \text{ \AA}$  is about the same as the diameter of the cavity in the oxygen layer of the “high-temperature” lattice model in Figure 1, so that it can just fit into one of these cavities and hence be difficult to replace (cf. “illitization”). For other cations it is the size of the hydrated ion that controls the replace-ability. Thus, for

ions of equal valence, those which are least hydrated have the greatest energy of replacement and are the most difficult to displace (Grim and Gueven, 1978). Typical CEC data of common smectite species are given in Table 4.

**Table 4: Typical CEC ranges for important smectites (After Pusch and Yong, 2006; Grim and Gueven).**

| Species         | CEC, meq/100 g |
|-----------------|----------------|
| Montmorillonite | 80-150         |
| Beidellite      | 80-135         |
| Nontronite      | 60-120         |
| Saponite        | 70-85          |

## 2.8 Anion sorption and replacement on smectite

Main mechanisms are:

Replacement of OH ions of particle surfaces,

1: Fitting onto the edges of the silica tetrahedral sheets and growing as extensions of these sheets. Other anions, such as sulfate and chloride, do not fit that of the silica tetrahedral sheets,

2: Local charge deficiencies can form anion-exchange spots on basal plane surfaces. This effect is assumed to be dominant in smectites, giving an anion exchange capacity of 5-10 meq/100 g.

## 2.9 Non-expanding minerals in smectite clays

Other clay minerals, rock forming minerals, amorphous constituents and organic matter, like bacteria, are present in various amounts. The most common non-expanding clay minerals are illite (hydrous mica, hydro-mica), chlorite, and kaolinite. Here, we will confine ourselves to give basic data on their hydration and sorption properties. They are commonly ascribed the following characteristic compositions (Pusch et al, 1995):

Illite:  $M^I_y Si_{(8-y)} Al_y O_{20} (OH)_4 (M^{III}, M^{II})_4$ , -

Chlorite:  $(Si, Al)_4 O_{10} (Mg, Fe, Al)_6 O_{10} (OH)_8$

Kaolinite:  $Si_2 Al_2 O_5 (OH)_4$ ,

where  $M^I$ = monovalent cations ( $K^+$  in illite),  $M^{II}$ = Mg and  $Fe^{3+}$ ,  $M^{III}$ = Al and  $Fe^{2+}$ .

These compositions imply different intraparticle bond strengths and hence different particle dimensions, which affects the specific surface area and the hydration potential. The crystal structure of the three clay mineral types is shown schematically in Figure 12.

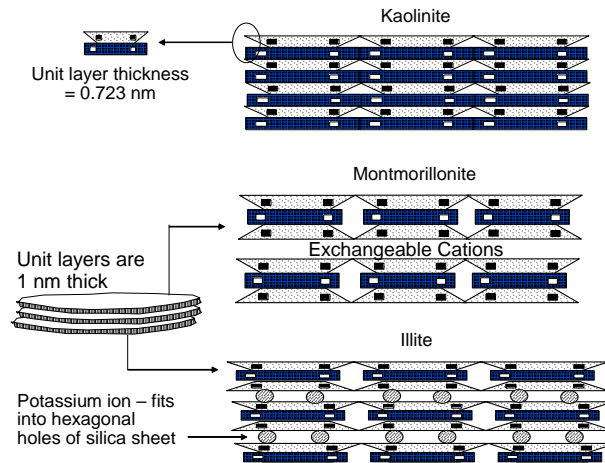


**Figure 12: Kaolinite, montmorillonite and illite minerals, using the simplified crystal notation given previously. In illite and montmorillonite cation substitution of Si for Al is common in the SiO layer, and of Al for Fe and other cations in the Al-O-OH layer.**

### 3. Quantification of clay microstructure by microscopy

#### 3.1 General

In the present context micrographs are those that can be used for explaining bulk behaviour of the clay in question and for correlating its constitution with its physical properties. In this regard, the arrangement and orientation of differently sized particles and aggregates of particles as well as of the system of voids are essential. They can best be evaluated from micrographs of very thin sections such as those used in association with transmission electron microscopy (TEM). An example of this can be seen in the micrograph of impregnated and ultramicrotomy-cut smectitic clay shown in Figure 13. The dark parts represent the most electron-sorbing objects, i.e. dense rock-forming minerals, and the brightest portions represent voids filled with impregnation resin for preparing ultrathin sections. The various degrees of greyness are clay gels of different density (Pusch, 1999).

Experience has shown that it is more useful to focus on the fraction of a section that is represented by voids since this refers to the permeable part of the clay. As indicated by Figure 13 one can identify dense and soft parts of the particle network as well as voids that are completely open. Their respective fractions of the analyzed part of the section can be determined with the aid of automatic scanning of digitalized versions of the micrographs. This makes it possible to distinguish between dense and impermeable parts of the clay, medium dense low-permeable parts, and open very permeable parts. From the viewpoint of hydraulic

conductivity one can generalize the microstructural pattern to consist of low-permeable and high-permeable parts as in the figure.

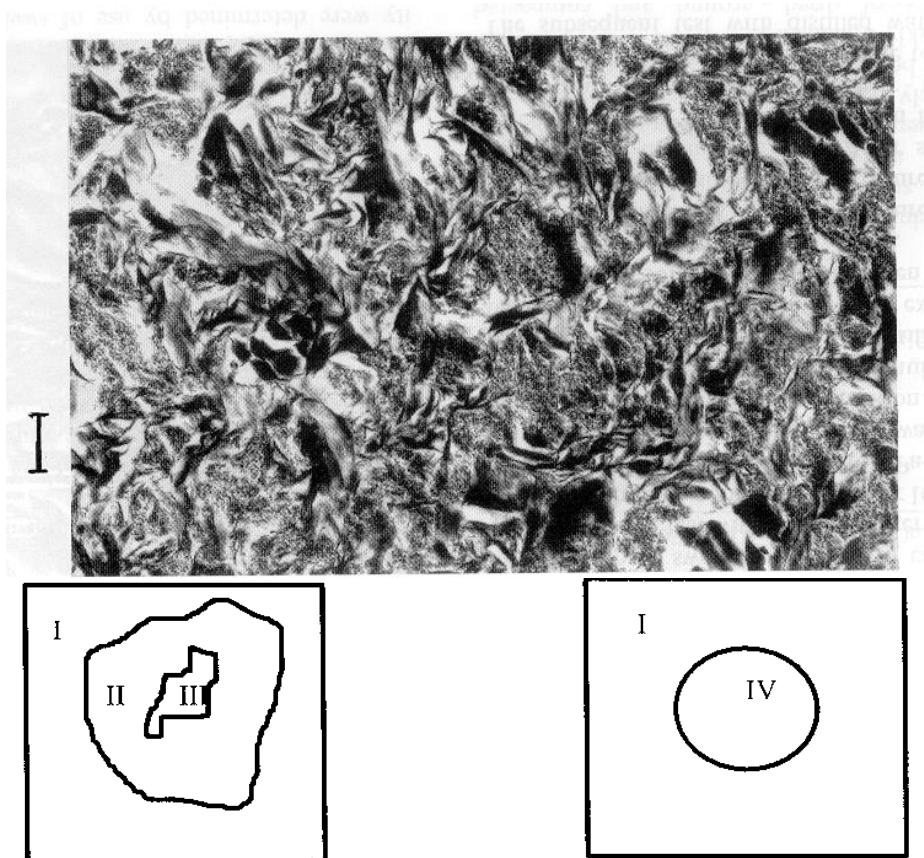


**Figure 13: Upper: TEM micrograph of 500 Å ultrathin section of clay with about 50 % expandable minerals and 1900 kg/m<sup>3</sup> bulk density at water saturation (dry density 1430 kg/m<sup>3</sup>). Darkest parts are minerals, while white parts are open voids. The bar is 1 μm long. Lower left: Soft matrix (I to III). Lower right: Channel section (Pusch, Muurinen et al, 1999).**

Useful microstructural parameters introduced some decades ago were the size (maximum diameter) of discernible voids, and the P/T ratio with P representing the sectioned voids, i.e. IV in the right picture in Figure 13, and T = the total section area. The latter can be correlated to the bulk hydraulic conductivity of natural clays deposited in fresh or salt water. Statistical treatment can be made of suitably defined microstructural parameters, taking the solid clay matrix to consist of two major components (Pusch et

al, 2006), i.e. 1) stacks, stack aggregates and non-smectite grains (*a*), and 2) gel-filled voids and unfilled voids (*b*). This distinction is made on the ground that the first-mentioned component is completely or largely impermeable while the latter offers little or no flow resistance. A further reason is that component *a* is largely responsible for the swelling pressure. Ion migration in this component takes place by both pore and surface diffusion. On the other hand, ion migration in *b*-space is almost entirely by pore diffusion. The two microstructural components are related through the coefficients  $F_2$  for 2D and  $F_3$  for 3D conditions and their ratio depends on the average and individual bulk densities as defined in Figure 14 and exemplified in Figure 15 for Wyoming bentonite. This procedure for density-related microstructural characterization can be applied to any soil analyzed with respect to the microstructural constitution using micrographs of very thin sections.

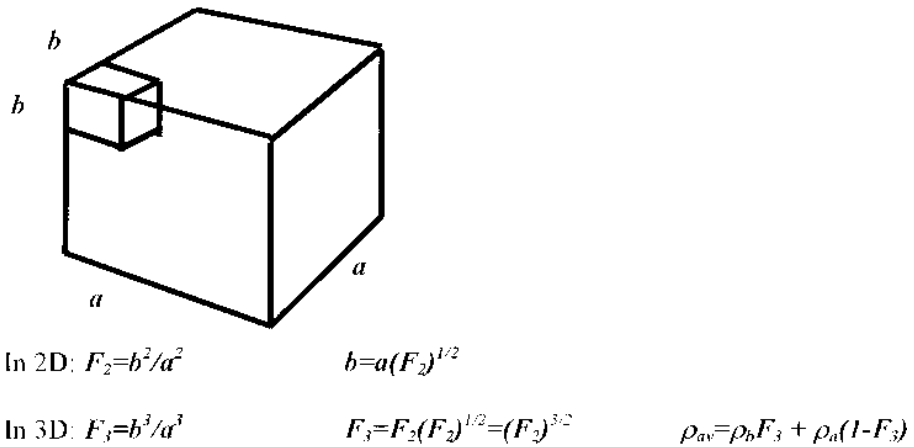


**Figure 14: Way of defining microstructural features in 2D and 3D.  $\rho_{av}$  is the “average” bulk density of the clay and  $\rho_a$  and  $\rho_b$  the average density of components *a* (stacks, stack aggregates and non-smectite minerals) and *b* (soft gel fillings and open space).**

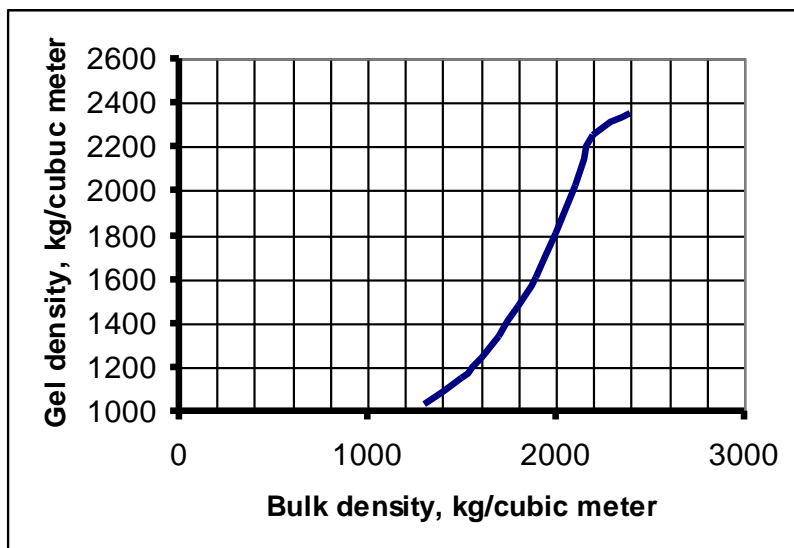


**Figure 15: Correlation of the average gel density ( $\rho_b$ ) and the average bulk density ( $\rho_{av}$ ) for Wyoming bentonite (MX-80).**

$F_2$  and  $F_3$  can be evaluated from digitalized TEM micrographs with different degrees of greyness representing different densities. They can be converted into different colours for easy interpretation and representation of the variation of density.

An example of a processed picture is shown in Figure 16. Using only four colours, clear distinction can be made of parts representing different densities: black parts, i.e. the most electron-absorbing components being the densest parts of component  $a$ , and red parts relatively dense parts of the same component. Green parts are taken as soft, porous parts of component  $b$ , and white representing open parts of this component. Depending on the scale,  $a$  or  $b$  may dominate and the matter of REV then becomes important. Thus, focusing on open voids and soft gels at high magnification gives very high  $F_2$  and hence also  $F_3$ -values, while focusing on dense aggregates gives very low  $F_2$  and  $F_3$ . For smectite-rich clays micrographs with an edge length of at least 30  $\mu\text{m}$  seem to be representative for the larger part of the clay matrix.  $F_2$  and  $F_3$  are related to the average bulk density of the clay as illustrated in Figures 16 and 17.

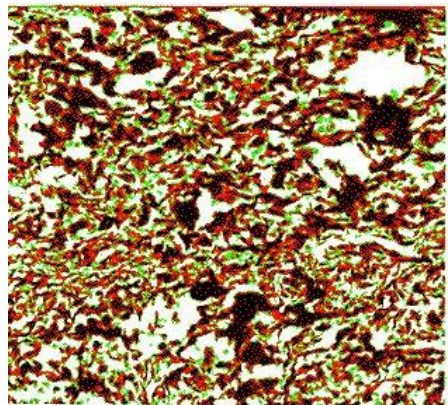


**Figure 16:** Example of digitalized micrograph of Wyoming bentonite (MX-80) with a bulk density at saturation of  $1800 \text{ kg/m}^3$  (dry density  $1270 \text{ kg/m}^3$ ). Black=densest parts of clay matrix *a*. Red=relatively dense parts of the same component. Green=soft, porous parts of component *b*. White representing open parts of this component. Edge length of micrograph is  $3\mu\text{m}$ .

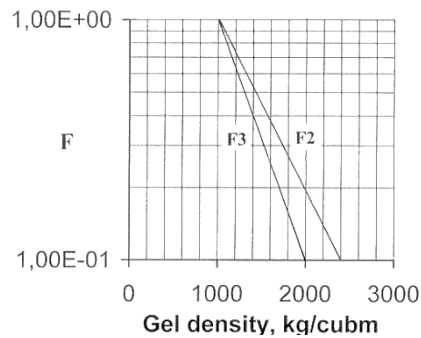


**Figure 17:** *F2* and *F3* versus gel density for Wyoming bentonite (MX-80). Data based on microstructural analyses using  $300\text{-}400 \text{ \AA}$  ultramicrotomed sections.

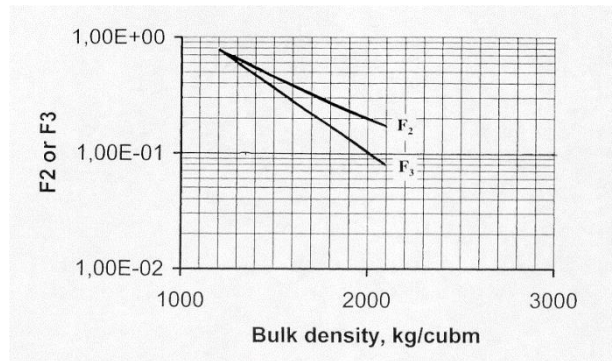


**Figure 18:  $F_2$  and  $F_3$  versus bulk density for Wyoming bentonite (MX-80).**

From such diagrams analytical expressions of parameters  $F_2$  and  $F_3$  can be derived as functions of the bulk density at saturation  $\rho_{bs}$  and the gel density  $\rho_{gs}$ . We will show here how these microstructural parameters are related to the hydraulic conductivity and swelling pressure.

### 3.2 Representativeness

For quantifying microstructural components like  $a$  and  $b$ , which represent density variations, one needs to find out how the section thickness affects the possibility of identifying microstructural features.

A practical way of doing this is to determine how the “grayness” of the micrographs is related to the density of the specimens. Dark parts are very energy-adsorbing microstructural components like solid non-smectite minerals, while medium-dark parts represent less dense clay aggregates and very bright parts represent voids filled with impregnation plastic. Intermediate degrees of grayness represent clay substance of different density. Figure 19 illustrates the need for preparation of very thin sections.

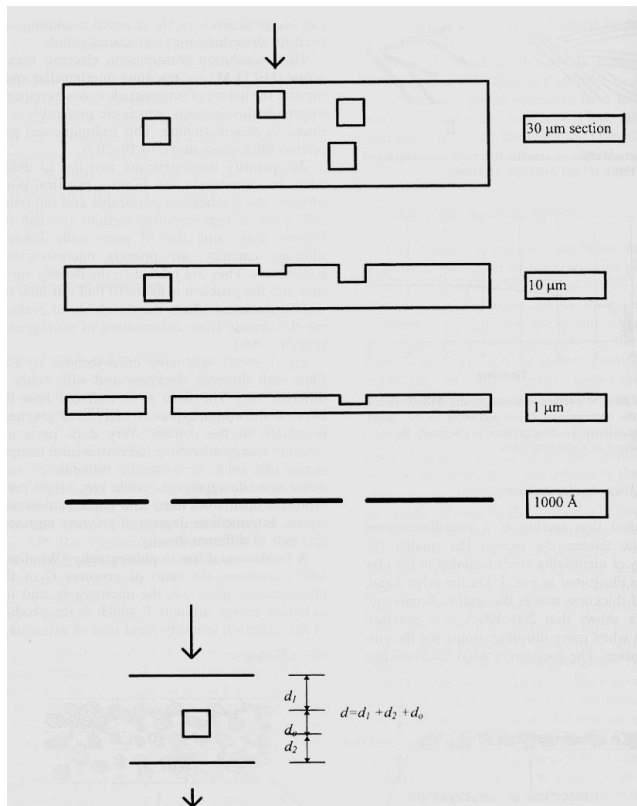


**Figure 19: The microtome-cut section thickness affects the microstructural interpretation: too thick sections do not reveal fine features. The bottom drawing shows a void element in the electron beam.**

### 3.3 Evaluation of “greyness”

A fundamental law in photography expresses the ratio of greyness  $G$  of the photographic plate, i.e. the micrograph, and the radiation energy amount  $E$ , which is the product of the radiation intensity  $i$  and time of exposure  $t$ :

$$G = A E = \log it \quad (3)$$

where:

$G$  = greyness

$A$  = constant

$E$  = radiation energy

$i$  = radiation intensity

$t$  = time of exposure

The greyness  $G$  is inversely proportional to the density  $\rho$  and thickness  $d$  of the film, which, for constant  $i$  and  $t$ , gives the expression:

$$G = B(\rho d)^{-1} \quad (4)$$

where:

$B$  = constant

$\rho$  = density

$d$  = film thickness

Disregarding from diffraction, optical distortions and radiation absorption by the void-filling impregnation substance, the intensity of the greyness of the micrograph on the exit side of the discrete element in Figure 19 is:

$$G = B [\Sigma (\rho d)]^{-1} \quad (5)$$

Comparing a section with 3  $\mu\text{m}$  thickness with one having 30  $\mu\text{m}$  thickness the ratio of the  $G$ -values is 10. In order to have direct quantitative comparison of the  $G$ -values, the radiation energy must be 10 times higher for the 30  $\mu\text{m}$  film thickness. This may have an impact on the crystal lattice stability, especially the location of alkali ions in EDX analyses.

While identification of the most detailed features of clay crystallites requires a resolution power that only sections thinner than 500-1000  $\text{\AA}$  can provide, certain quantitative microstructural analyses can be made by using significantly thicker films. For artificially prepared smectite clays using clay powder that hydrates under confined conditions, sufficient information may be obtained by examining

10  $\mu\text{m}$  sections. Hence, clays of this sort with a density of 1700 to 2000  $\text{kg/m}^3$  at water saturation are commonly characterized by the presence of one 3-5  $\mu\text{m}$  wide zone of soft gels per 1000  $\mu\text{m}^2$  cross section area. Such a zone located in the center of the section in the lower drawing in Figure 19 would mean that the thickness of the dense matrix ( $d_1 + d_2$ ) can be about 50 % of that of the surrounding homogeneous clay matrix. The greyness of the micrograph where the channel is located would then be 50 % of that of the rest of the section. This is sufficient to indicate the presence of such a channel or local void. However, no detailed information on the zone can be obtained and one cannot distinguish between a case with one void and cases with two or several thinner voids located on top of each other. A 30  $\mu\text{m}$  clay film gives even less information on density variations while sections with a thickness of about 5  $\mu\text{m}$  provide considerably more information on density variations.

Micrographs of sections with 1  $\mu\text{m}$  thickness provide very detailed information on the microstructural constitution.

More advanced interpretation of micrographs that has revealed other microstructural features like channeling has been made in the last few years (Bouchelaghem and Pusch, R., 2017). Such a step to further directly correlate the microstructural constitution of smectite clay with lab investigations was recently made by Bouchelaghem and Pusch (2017). They modelled the hydraulic transmission of coupled “2D” TEM electron images by using the technique of “Homogenization of Periodic Media”, distinguishing between three levels: the microscopic level of clay particles, the mesoscopic level of clay aggregates, mineral grains and inter-aggregate porosity, and the macroscopic level of the sample subjected to hydraulic conductivity tests in the laboratory. Several cases were distinguished as soft and dense gels, open voids forming connected flow paths, or remaining occluded. For all three cases considered, starting from the local description of fluid flow, expressions of the effective hydraulic conductivity tensor were derived. The microstructure was obtained by image analysis of digitalized micrographs in order to obtain the contours of the different phases. These contours were then imported into a finite element-based software in order to solve the local problems. Numerical computations allowed the authors to investigate the contribution to macroscopic flow by the soft and dense gels in connected and non-connected configurations (cf. Figure 20). The study strongly supports the applicability of a similar model for through-flow of smectite-rich clay, considered as a system of gel-filled channels of different size, using the 3Dchan code worked out by Neretnieks and Moreno (1993), and has been successfully used by the present author for modelling flow through soft, medium-dense and dense smectite clays (Pusch et al, 2001).

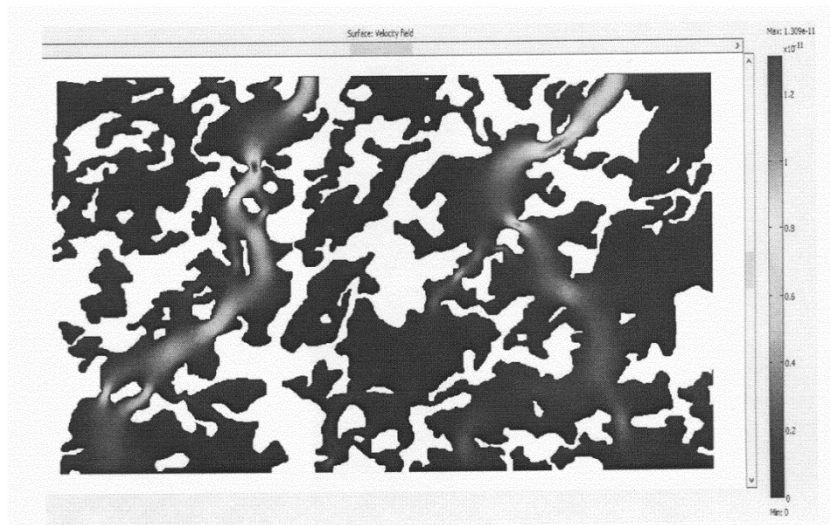


**Figure 20: Steps in calculating the hydraulic conductivity by use of 2D digitalized electron micrographs (Bouchelaghem and Pusch, 2017): Identified connected macropores making up microstructural channels. Vertical scale represents the distribution of the hydraulic conductivity.**

As stated earlier in the paper micrographs of smectite clay are representative for the larger part of the clay matrix and the parameters.  $F_2$  and  $F_3$  are related to the average bulk density of the clay as illustrated in Figures 16 and 17: micrographs of smectite-rich clays with an edge length of at least 30  $\mu\text{m}$  seem to be representative for the larger part of the clay matrix.  $F_2$  and  $F_3$  are related to the average bulk density of the clay as illustrated in Figures 16 and 17.

Focusing first on the use of the  $F$  parameters for checking the relevance and usefulness of the procedure for quantifying microstructure by comparing experimentally obtained bulk hydraulic conductivity data for Na and Ca smectite clay, we will use the system of elements with different hydraulic conductivities in Figure 21.

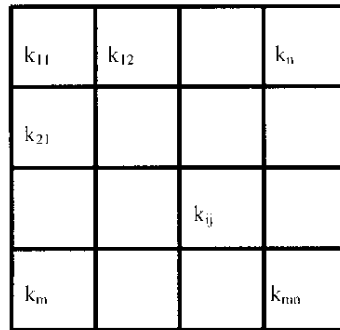


**Figure 21: System of elements with different hydraulic conductivity permeated in horizontal direction.**

The mean hydraulic conductivity  $K$  of clay with elements of different conductivity can be expressed as follows:

$$K = 1 / m \left[ \sum_{i=1}^m n \left\{ \sum_{j=1}^n 1 / k_{ij} \right\} \right]^{-1} \tag{6}$$

where:

$K$ = average hydraulic conductivity

$n$ = number of elements normal to flow direction

$m$ = number of elements in flow direction

$k_{ij}$ = hydraulic conductivity of respective element

The cross-sectional areas of individual voids identified in micrographs, together with the corresponding  $K$ -value calculated from Equation (6) have been compared with experimentally obtained data, and found to agree satisfactorily. Considering the uncertainty in estimating interconnectivity and tortuosity of the gel-filled voids and channels, and distinguishing only between permeable and impermeable fractions of the sections as a first order simplification, it appears to be reasonable. The fraction  $F_2$  representing the permeable gel-filled fraction of REV sections can thence be used for calculating  $K$ . The conductivity of the clay gels is assumed to be similar to the experimentally determined conductivity of clay with the same bulk density.  $F$ -data together with the calculated  $K$ -values are shown in Tables 5 and 6 for three representative bulk densities. Good agreement is obtained between the model-derived data for artificially prepared Wyoming clay (MX-80) in Na form and experimentally determined results.

**Table 5: Microstructural data and conductivities [m/s] for MX-80 in Na form.  
Percolation with distilled water.**

| <b>Bulk density, [kg/m<sup>3</sup>]</b> | <b>F<sub>2</sub></b> | <b>Gel density [kg/m<sup>3</sup>]</b> | <b>Gel conductivity</b> | <b>Calculated bulk conductivity</b> | <b>Experimental bulk conductivity</b> |
|---|----------------------|---------------------------------------|-------------------------|-------------------------------------|---------------------------------------|
| 2130 Na                                 | 0.17                 | 2000                                  | 7E-14                   | E-14                                | 2E-14                                 |
| 1850 Na                                 | 0.24                 | 1650                                  | 2E-12                   | 4E-13                               | 3E-13                                 |
| 1570 Na                                 | 0.40                 | 1150                                  | 2E-10                   | 8E-11                               | 8E-11                                 |

The microstructural heterogeneity of the artificially prepared MX-80 clay is a significant factor for the hydraulic conductivity of the clay. In comparison to natural sedimentary clays with the same density and smectite content, the results indicate that higher hydraulic conductivity values are obtained for the artificially prepared MX-80 clay. The reason is that the latter will undergo further homogenization by creep and chemically induced changes in the time perspective of thousands of years in order to represent “natural” sediments.

Implication of cation exchange is as follows from the perspective of double-layer interaction (DDL): interactions within the lamellae by cation replacement of Na<sup>+</sup> by Ca<sup>2+</sup> will raise the hydraulic conductivity. Assuming the same  $F_2$  values and gel densities as for MX-80 in Na form, and gel conductivities for MX-80 in Ca form, one obtains the data in Table 6, which gives the density of Na-MX-80 bulk density in the first column, while the data in other columns refer to MX-80 in Ca form.

**Table 6: Microstructural data and conductivities [m/s] for MX-80 in Ca form. Percolation with strongly brackish Ca-dominated water (Pusch and Yong, 2006).**

| Bulk density, [kg/m <sup>3</sup> ] | F2   | Gel density [kg/m <sup>3</sup> ] | Gel conductivity | Calculated bulk conductivity | Experimental bulk conductivity |
|------------------------------------|------|----------------------------------|------------------|------------------------------|--------------------------------|
| 2130 Na                            | 0.17 | 2000                             | 2E-13            | 3E-14                        | 3E-14                          |
| 1850 Na                            | 0.24 | 1650                             | 8E-11            | 2E-12                        | 2E-12                          |
| 1570 Na                            | 0.40 | 1150                             | 7E-5             | 3E-06                        | 2E-09                          |

One finds that there is good accord between calculated and true conductivity data for bulk densities as low as about 1800 kg/m<sup>3</sup> (dry density 1270 kg/m<sup>3</sup>). The role of cation exchange on the hydraulic conductivity is also well demonstrated by the results portrayed in Figure 22 for tests on MX-80 with this density, where the permeating fluid consisted of 3.5% CaCl<sub>2</sub> solution. The initial rise in hydraulic conductivity was due to the rinsing effect of dislodgement of particles. However, these particles, together with the resultant non-homogeneous gel formation in the voids, then became void pluggers. When this occurred, a deterioration in the hydraulic conductivity took place as witnessed by the drop in the hydraulic conductivity after one day (Pusch and Yong, 2006).

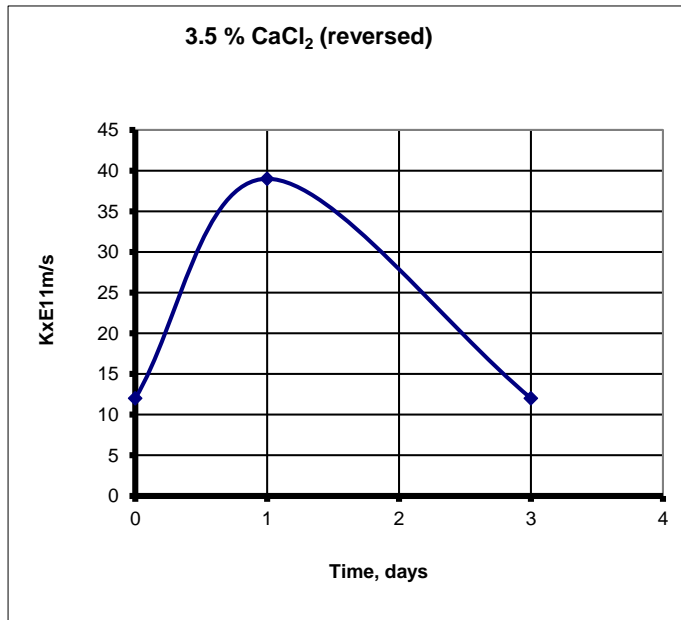


**Figure 22: Change in hydraulic conductivity of a smectite-rich clay with a density of 1800 kg/m<sup>3</sup> at saturation (1270 kg/m<sup>3</sup> dry density) followed by reversal flow with 3.5 % CaCl<sub>2</sub> solution under a hydraulic gradient of 30 m/m. The conductivity initially increased in conjunction with disruption of soft clay gels, and subsequently dropped because of accumulation of released particles at channel constrictions.**

### 3.4 Expandability

#### 3.4.1 Swelling pressure

The swelling pressure exerted on the physical boundaries of smectite clay seals is caused by combination of true “disjoining” pressure caused by the interlamellar water films, which strive to grow to a certain finite thickness if expansion can take place, and of the osmotic pressure caused by the charge conditions at the outer boundaries of the stacks of lamellae.

The swelling pressure-time relationship shown in Figure 23 has been obtained from swelling pressure tests on montmorillonite-rich clay, using oedometers equipped with stiff pressure cells. The clay sample was prepared by compacting air-dry clay powder directly in the oedometer, and then allowed to take up water. For a smectite-rich clay with a dry density of at least a few hundred kg/m<sup>3</sup> the air enclosed in the powder becomes pressurized in the hydrating clay. The air

dissolves and diffuses out of the system – a process that occurs even if water uptake is allowed to occur from only one end. The first peak reached after the first day is due to evolution of the microstructure. From a physical standpoint, we can describe this as the expansion process of the individual dense clay granules and subsequent movement into more stable positions of aggregates and individual particles. This process is by no means complete in the early days because the process of expansion depends on water uptake rate, which is a slow process. In consequence, continuous readjustment of the expanding and expanded granules to more stable positions occurs.

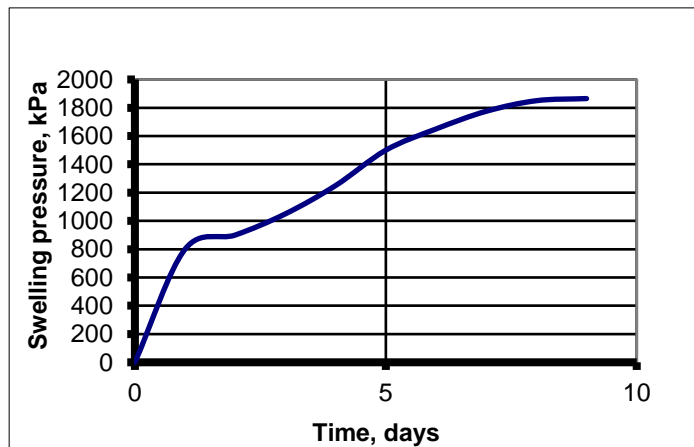


**Figure 23: Development of swelling pressure of maturing clay with montmorillonite content of about 70 % and a dry density of  $1390 \text{ kg/m}^3$  ( $1875 \text{ kg/m}^3$  at complete saturation). The sample was prepared by compression of air-dry MX-80 clay granules followed by saturation with distilled water.**

Typical smectite swelling pressure data are collected in Table 7.

**Table 7: Swelling pressure ( $p_s$ ) in MPa of well characterized smectite-rich materials at saturation with distilled water. (S= smectite, I=Illite). (1800 and 2000 kg/m<sup>3</sup> total density correspond to the dry densities 1270 kg/m<sup>3</sup> and 1590 kg/m<sup>3</sup>, respectively) (“Friedland clay”)**

| Density at Saturation [kg/m <sup>3</sup> ] | 1800    | 2000 |
|--|---------|------|
| MX-80                                      | 0.8-0.9 | 4-5  |
| IBECO, Na                                  | 0.6-1   | 4-5  |
| IBECO, Ca                                  | 0.2     | 5    |
| Beidellite                                 | 1.5     | 4.2  |
| Saponite                                   | 2.5     | 8.8  |
| Mixed.l. S/I (*)                           | 0.1     | 0.9  |
| *Friedland clay                            |         |      |

The smectite-rich clays MX-80 and IBECO, which are commercially available in large quantities, have montmorillonite as major smectite constituent (75-90%). Saponite and beidellite behave as montmorillonite for low densities while they develop higher swelling pressures at high densities. For densities higher than about 2000 kg/m<sup>3</sup> at fluid saturation, the chemical composition of the pore water does not exercise much influence on the swelling pressure because the DDL forces are practically non-existent. The low amount of water uptake at very high densities is to all intents and purposes structured pseudo-crystalline interlamellar water. Water uptake beyond hydrate water will be by DDL forces, at which time the density of the samples will be considered in the medium density range and the influence of the cation species becomes significant. For lower densities, the chemical composition of the pore water is very important.

In this context it is worth mentioning that Friedland clay with its dominant content of mixed-layer smectite/muscovite is less affected by variations in pore water chemistry than the smectite-rich clays and the pressure is lower at all densities. This is attributable to the lower expandability of the crystal lattice and the lower content of clay gels in the voids between dense, expanded granules. One should note that for a smectite-rich clay with 1350 kg/m<sup>3</sup> dry density saturation with brine of 20 % NaCl will develop a swelling pressure of at least 100 kPa. This is considered to be a minimum requirement for supporting the roof of backfilled tunnels and drifts in repositories.

We will not comment on gas permeability here other than that experience (Osipov et al, 2004) and comprehensive gas migration tests indicate that gas penetration and transport in smectite clay is related to the swelling pressure, which has to be

exceeded for letting pressurized gas through (Pusch, et al, 1985; Horseman and Harrington, 1997; Wilson et al, 2011).

### 3.4.2 Relevance and use of $F$ -parameters

We have stated that the swelling pressure is caused by the disjoining forces in the inter-lamellar space and double-layer repulsion. Considering the actual force distribution in the common heterogeneous microstructure, the swelling pressure is seen to be proportional to the product of the true swelling pressure of the pressure-controlling component  $a$  and the volume ratio  $(a^3-b^3)/a^3$  in Figure 14. This ratio is  $(1-F_3)$ , which gives the volume fraction of this component. For a bulk density of  $2130 \text{ kg/m}^3$   $\rho_a$  is  $2000 \text{ kg/m}^3$  and the true swelling pressure of this component, calculated using the Yong and Warkentin theory, is about 11 MPa, assuming isotropic distribution and orientation of the smectite lamellae. The value of  $(1-F_3)$  is 0.93 and, in consequence, the product is about 10 MPa. For the bulk density  $1570 \text{ kg/m}^3$   $\rho_a$  is  $1750 \text{ kg/m}^3$ , and the true swelling pressure about 0.3 MPa. The value of  $(1-F_3)$  is 0.75 and the product is about 0.2 MPa. The values are in good agreement with experimental data as illustrated by Table 8.

**Table 8: Calculated and experimentally determined swelling pressures ( $p_s$ ) of MX-80 saturated with distilled water.**

| Bulk density [kg/m <sup>3</sup> ] | 1-F <sub>3</sub> | Density of massive part [kg/m <sup>3</sup> ] | $p_s$ of massive part, [MPa] | Calculated bulk $p_s$ [MPa] | Experimental bulk $p_s$ [MPa] |
|-----------------------------------|------------------|--|------------------------------|-----------------------------|-------------------------------|
| 2130                              | 0.93             | 2150   | 15                           | 14.0                        | 14                            |
| 1850                              | 0.80             | 1900   | 1.5                          | 1.2                         | 1.0                           |
| 1570                              | 0.75             | 1750   | 0.5                          | 0.4                         | 0.3                           |

Applying the same generalization as for the hydraulic conductivity, i.e. assuming that the major microstructural features expressed in terms of  $F_3$ , are about the same as for saturation with distilled water, one has recorded for MX-80 in Ca form the same theoretical swelling pressure as for MX-80 saturated with distilled water when the bulk density is 1570, 1850 and 2130  $\text{kg/m}^3$ , respectively. These pressure values agree well with experimental results (Pusch and Yong, 2006; Herbert and Kasbohm, 2008). Even for the lowest density at saturation, 1570  $\text{kg/m}^3$  (dry density 900  $\text{kg/m}^3$ ) there is fair agreement but an indication of insufficient sensitivity of the simple model for densities representing conditions close to complete expansion of the densest part of the clay matrix ( $a$  in Figure 14). On altering the pore water electrolyte of smectite-rich clay with a density of 2130  $\text{kg/m}^3$ , from a low salinity solution to sea water, the swelling pressure was unchanged which is also as

documented by numerous experiments. For a bulk density of  $1850 \text{ kg/m}^3$  at saturation with distilled water the theoretical value would be about 1.2 MPa to be compared with the experimental value 1.0 MPa, while for sea water a typical experimental value is on the order of 0.5 MPa. For the lowest bulk density  $1570 \text{ kg/m}^3$  the dry density is 900 kPa and the theoretical swelling pressure about 0.15 MPa, while recorded swelling pressures are only a few tens of kPa. The influence of increased Na concentration in the porewater is similar to the effect obtained for hydraulic conductivity.

#### **4. Comments and conclusive remarks**

Smectite clay is used for isolating low- and intermediate-level radioactive waste in on-ground and relatively shallow underground repositories from the groundwater for a few hundred or thousand years Pusch (2008, 2012) and Svemar (2005). Highly radioactive waste that can give off cationic and anionic radionuclides can also be shielded by such clay at medium or large depth if the density is high. The clay seals need to be very dense for minimizing percolation and for providing a high enough swelling pressure that can generate self-healing of local parts with lower density. They have to remain largely impermeable for at least 100,000 years, and be sufficiently ductile to sustain seismic and tectonic impact that would otherwise cause breakage and leakage of the waste canisters. The clay seals are placed around and between waste packages. The objective of the present paper is to illustrate how simple modelling of the maturation of smectite clay seals can be made and how permeation of them takes place by increasing or decreasing the dry density.

We assume in this paper that engineering barriers of smectite clay maintain their chemical and mineralogical states for the required operational period of time, as long as the temperature does not exceed about  $60^\circ\text{C}$  at which it is assumed to become converted to a high-temperature form, implying reorganization of lattice hydroxyls. One understands from the described function of adsorbed cations that exchange of them from Na to Ca by flooding the repository with seawater has great impact on the physical performance of smectite clay seals with moderate density. The most important contribution to the understanding of the role of clay microstructure is the described way of interpreting transmission micrographs for substantiating the heterogeneity of the clay in a form that makes it possible to correlate microstructure and experimental bulk data respecting geotechnical properties of soils. It seems possible to further develop the technique for classifying soils by use of microstructural parameters.

The issue of diffusive ion transport is planned to be treated in a similar way as water permeation using the same or similar microstructural parameters and comprehensive laboratory data like those reported by Brandberg and Skagius (1991) for the Swedish Nuclear Fuel and Waste Management Co. A pilot study

was made by Pusch et al in the EU project Micro-structural and chemical parameters of bentonite as determinants of waste isolation efficiency (European Commission Final Report Contr. No. F14W-CT95-0012).

## References

- [1] Bouchelaghem, F. and Pusch, R. (2017). Clay microstructure: imaging numerical homogenization and correlation with physical data. *Applied Clay Science*, 144, 9-18.
- [2] Brandberg, F. and Skagius, K. (1991). Porosity, sorption and diffusivity data compiled for the SKB 91 study. Swedish Nuclear Fuel and Waste Management AB (SKB) Technical Report TR 91-16, SKB, Stockholm.
- [3] Colten, V.A. (1986). Hydration states of smectite in NaCl brines at elevated pressures and temperatures. *Clays and Clay Minerals* 1986 34, 385-389.
- [4] Horseman and S.T., Harringtonm, J. F. (1997). Study of gas generation in MX-80 buffer bentonite. British Geological Survey, WE197/7.
- [5] Kehres, A. (1983). Dehydration energy isotherms of clays. Diagrams for surfaces of interlamellar and extralamellar (microvoids) space. PhD Thesis Université Paul Sabatier, Toulouse, France.
- [6] Neretnieks, I. and Moreno, L. (1993). Fluid flow and solute transport in a network of channels, *Journal of Contaminant Hydrology*, 14, 163-192.
- [7] Osipov, V.I., Sokolov and V.N., Eremeev, V.V (2004). Clay seals of oil and gas deposits. Balkema Publishers, Lisse/Atingdon/Exton (PA)/Tokyp ISBN 90 5809 90 5809 583.
- [8] Pusch, R., Ranhagen, L. and Nilsson, K. (1985). Gas migration through MX-80 Bentonite. NAGRA Technical Report 85-36.
- [9] Pusch, R., Muurinen, A., Lehikoinen, J., Bors, J. and Eriksen, T. (1999). Micro-structural and chemical parameters of bentonite as determinants of waste isolation efficiency. European Commission Final Report Contr. No. F14W-CT95-0012.
- [10] Pusch, R. (1999). Clay colloid formation and release from MX-80 buffer SKB Technical Report TR-99-31. Swedish Nuclear Fuel and Waste Management Co(SK B), Stockholm, Sweden.
- [11] Pusch, R., Moreno, L. and Neretnieks, I. (2001). Microstructural modelling of transport in smectite clay buffer. *Proc. Int. Symp. On suction, swelling, Permeability and structure of clays*. Eds. K Adachi & M Fukue. Balkema, Rotterdam/Brookfield. ISBN: 90 5809 175 9.
- [12] Forslind, E. and Jacobsson, A. (1972). Clay water systems: in: *Water, a Comprehensive Treatise*. F. Franks (ed); Plenum Press, New York.
- [13] Herbert, H. J., Kasbohm, J., Sprenger, H., Fernández A.M. and Reichelt, C. (2008). Swelling pressures of MX-80 bentonite in solutions of different ionic strength. *Physics and Chemistry of the Earth*, 33, 327-342.

- [14] Neretnieks, I. and Moreno, L. (1993). Fluid flow and solute transport in a network of channels, *Journal of Contaminant Hydrology*, 14, 163-192.
- [15] Pusch, R. (1993). Evolution of models for conversion of smectite to non-expandable minerals. SKB Technical Report TR-93-33, SKB, Stockholm, Sweden.
- [16] Pusch, R. and Yong, R.N. (2006). Microstructure of smectite clays and engineering performance. Taylor & Francis, London.
- [17] Pusch, R. (2008). Geological storage of radioactive waste, Springer-Verlag, Berlin, Heidelberg, (ISBN: 978-3-540-77332-0).
- [18] Pusch, R. (2012). The geological basis for developing concepts for disposal of highly radioactive waste (HLW) in crystalline rock – a state of art compilation. *Communicaciones Geológicas*, vol. 99, no.1, 2012, 61-68.
- [19] Pusch, R. (2015). Bentonite Clay, Environmental Properties and Applications, CRC Press.
- [20] Sposito, G. (1984). The surface chemistry of soils. Oxford University Press, New York, Clarendon, Oxford.
- [21] Svemar, C. (2005). Cluster repository project (CROP). Final Report of European Commission Contract FIR1-CT-2000-20023, Brussels, Belgium.
- [22] Wilson, J., Savage, D., Bond, A., Watson, S., Pusch, R. and Bennett, D. (2011). Bentonite - A Review of key properties, processes and issues for consideration in the UK context. Quintessa Ltd., Henley-on-Thames, UK.